


# Non-invasive monitoring of cardiac contractility: Trans-radial electrical bioimpedance velocimetry (TREV)

Alexandra Stump<sup>1,†</sup>  | Caitlin Gregory<sup>1,2,†</sup>  | Viktoriya Babenko<sup>1</sup>  | Elizabeth Rizor<sup>1,2</sup>  | Tom Bullock<sup>1,2</sup>  | Alan Macy<sup>3</sup>  | Barry Giesbrecht<sup>1,2</sup>  | Scott T. Grafton<sup>1,2</sup>  | Neil M. Dundon<sup>1,2,4</sup> 

<sup>1</sup>Department of Psychological and Brain Sciences, University of California, Santa Barbara, California, USA

<sup>2</sup>Institute for Collaborative Biotechnologies, University of California, Santa Barbara, California, USA

<sup>3</sup>BIOPAC Systems, Inc, Goleta, California, USA

<sup>4</sup>Department of Child and Adolescent Psychiatry, Psychotherapy and Psychosomatics, University of Freiburg, Freiburg, Germany

## Correspondence

Neil M. Dundon, Department of Psychological and Brain Sciences, University of California, Santa Barbara, CA 93106, USA.

Email: [neil.dundon@psych.ucsb.edu](mailto:neil.dundon@psych.ucsb.edu)

## Funding information

Institute for Collaborative Biotechnologies under Cooperative Agreement, Grant/Award Number: W911NF-16-1-0474, W911NF-19-D-0001 and W911NF-19-2-0026; Army Research Office

## Abstract

We describe methods and software resources for a bioimpedance measurement technique, ‘trans-radial electrical bioimpedance velocimetry’ (TREV) that allows for the non-invasive monitoring of relative cardiac contractility and stroke volume. After reviewing the relationship between the measurement and cardiac contractility, we describe the general recording methodology, which requires impedance measurements of the forearm. We provide open-source Jupyter-based software (operable on most computers) for deriving cardiac contractility from the impedance measurements. The software includes tools for removing variance associated with heart rate and respiration. We demonstrate the ability of this bioimpedance measurement for tracking beat-to-beat changes of contractility in a maximal grip force production task. Critically, the results demonstrate both a reactive increase in contractility with force production, and suggest there is a learned increase in contractility prior to grip onset, consistent with anticipatory allostatic autonomic regulation mediated by sympathetic inotropy. The method and software should be of broad utility for investigations of event-related cardiac dynamics in psychophysical studies.

## KEYWORDS

allostasis, analysis/statistical methods < methods, autonomic < methods, cardiovascular < methods, effort and mobilization, motor control < content/topics, stress, unconscious processes < content/topics, young adults < groups studied

## 1 | INTRODUCTION

The cardiovascular system adapts quickly and dynamically in anticipation of and in response to a variety of mental and physical conditions. Tracking these

perturbations by a measurement with high temporal resolution is a promising approach for identifying physiological responses to psychological drivers such as motivation, challenge, coping or stress as well as physical demands (Blascovich, 2013; Cieslak et al., 2018; Obrist, 1981; Richter

<sup>†</sup>Alexandra Stump and Caitlin Gregory contributed equally as first author.

This is an open access article under the terms of the [Creative Commons Attribution-NonCommercial-NoDerivs](https://creativecommons.org/licenses/by-nc-nd/4.0/) License, which permits use and distribution in any medium, provided the original work is properly cited, the use is non-commercial and no modifications or adaptations are made.

© 2023 The Authors. *Psychophysiology* published by Wiley Periodicals LLC on behalf of Society for Psychophysiological Research.

& Gendolla, 2009). Bioimpedance methods, particularly impedance cardiography (ICG), have long been used to investigate modulation of the autonomic nervous system to the heart by capturing electromechanical modulation of cardiovascular activity during cognitive tasks (Miller & Horvath, 1978). ICG uses a high-frequency electrical current typically delivered with as few as four electrodes placed on the neck and thorax, while additional electrodes are required to record the electrocardiogram. Using the combination of impedance cardiography and electrocardiography, a number of cardiodynamic parameters can be derived. These include intervallic electromechanical parameters such as the pre-ejection period (PEP) as well as estimates of left ventricular ejection time (LVET), stroke volume (SV) and cardiac output (CO) based on idealized models of the thorax (Bernstein, 2009; Trakic et al., 2010).

While ICG is a powerful approach, the method has drawbacks. There are diverse physiologic and anatomic sources that influence changes in thoracic impedance, undermining the ability to estimate peak aortic blood flow, an indicator of contractility (Wang & Patterson, 1995). Because the measurements are acquired across the thorax, the normal respiratory cycle introduces additional confounds due to changes of thoracic size and shape that undermine the application of ideal models. Pragmatically, operational challenges related to applying electrodes to the naked torso pose additional limitations. More problematic has been the modelling of the resultant thoracic impedance waveform. The analysis depends on the identification of the b-point, a subtle inflection of the thoracic impedance wave corresponding to the opening of the aortic valve. Despite the development and distribution of semi-automated software tools by our laboratory for expediting the labelling of the b-point, we find that for many studies b-point identification continues to require extensive hands-on expert quality control for labelling ambiguous time points. While the variability in labelling the b-point can be overcome by averaging heartbeats over a sliding time window, this compromises the goal of measuring alterations of PEP, LVET or SV on a fast time scale (Cieslak et al., 2018).

Given the challenges that ICG analysis presents for the estimation of cardiac contractility, we have investigated other bioimpedance measurement techniques. Here we present a particularly promising method called trans-radial electrical bioimpedance velocimetry (TREV) (Bernstein et al., 2012). TREV is a user-friendly approach that measures impedance signals along the length of the volar forearm. Changes of the impedance signal are directly related to a pressure/pulse wave propagating along the radial and ulnar arteries that arises after the opening of the aortic valve. In the following sections, we review the factors that influence contractility, and then describe

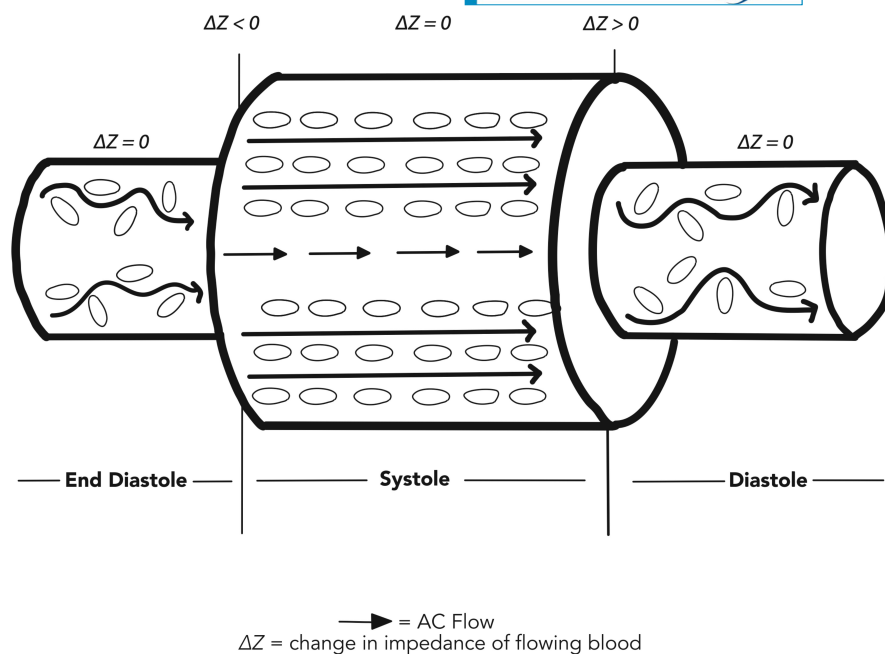
the underlying biomechanical and electrical properties of TREV that lead to the estimation of cardiac contractility. We note that while others have measured bioimpedance in the periphery, specifically in the leg, their experimental goal was to estimate blood velocity and peripheral vascular compliance through simultaneous acquisition of thoracic bioimpedance (Sel et al., 2021). A key innovation of TREV is to derive the peak acceleration of the impedance wave, which directly relates to peak aortic pulse pressure and hence, end systolic intraventricular pressure, a proxy of contractility. We demonstrate the utility of TREV with an isometric grip force task to capitalize on the known increase in contractility while humans apply a brief maximum force to a grip transducer (Stanek & Richter, 2016; Stanek & Richter, 2021). From this, we present preliminary evidence that TREV is capable of capturing beat-by-beat allostatic anticipatory changes in contractility. The observed contractility changes are independent of heart rate increases and cyclic respiration, suggesting that participants can learn to develop increased sympathetic drive to the heart prior to hand grip onset. Finally, we provide an appendix describing signal processing software, amalgamating multiple python packages (Gramfort et al., 2013; Hunter, 2007; Vack, 2023; Virtanen et al., 2020), and operable on most computers, and a tutorial for streamlining the conversion of TREV impedance measurements into beat-by-beat estimates of contractility.

## 1.1 | Background physics and physiology

### 1.1.1 | Red blood cells and impedance

Several biophysical properties contribute to the changes of electrical impedance measured with TREV. Under static conditions (without blood flow or arterial pressure gradients but with constant blood volume and constant alveolar gas partial pressure), the red blood cells, constituting approximately 40% of blood volume in a vessel, will be randomly oriented. Due to the random orientation of the biconcave red blood cells, an increased resistance within the plasma is observed and the artery exhibits a maximal level of electrical resistivity measurable as impedance  $Z$  in units of Ohms ( $\Omega$ ) (Bernstein, 2009). In contrast, when blood flow traverses the radial and ulnar arteries, the short axis of red blood cells aligns perpendicularly to the flow axis, leading to a decrease in impedance (Figure 1). This impedance signal  $Z$  depends on both blood velocity ( $v$ ) and blood volume. If these are held constant (as in physics), then measured impedance  $Z$  remains in units of  $\Omega$ . Yet, because each heartbeat causes blood to flow and experiences a pressure wave the measured impedance  $Z$  becomes a dynamic, as opposed to a static (as in physics)

**FIGURE 1** Alterations in red blood cell orientation and impedance during pulsatile blood flow through the artery of the forearm. During systole, the pressure wave both dilates the blood vessel and rapidly aligns red blood cells, resulting in decreased impedance. Adapted from Bernstein (2009).



measure. Therefore, it is appropriate to report  $Z$  in physiology studies in units of  $\Omega/s$  (Bernstein et al., 2012). As shown in Figure 1 there is a potential for blood volume to increase with each heartbeat. While this clearly occurs in the proximal aorta (the windkessel phenomenon), ultrasound-measured pulsatile changes of blood volume in the upper arm and forearm vasculature are negligible (Chuang et al., 2002; Green et al., 2002; Lott et al., 2002).

### 1.1.2 | Peak acceleration of blood and impedance

During diastole of the cardiac cycle, the aortic valve is closed, isolating aortic blood pressure from intraventricular pressure as blood fills the ventricle, boosted by atrial contraction. With systole, the ventricular myocardium contracts, the mitral valve closes and isovolumic intraventricular pressure rapidly rises until pressure in the ventricle surpasses aortic pressure, at which point the aortic valve opens. A pressure surge is transmitted into the aorta leading to a rapid rise in proximal arterial blood velocity. Distally, the pulse pressure in the radial artery is approximately 1/3 of the peak pressure generated by the heart. Continuous flow is dependent on the compliance of the proximal aorta which expands and then contracts during systole (windkessel). Mean velocity is affected by the downstream tapering of the peripheral arteries, where the pulse pressure encounters reduction in vessel compliance and time varying increased elastance  $\Delta P/\Delta V$ , which are caused by progressive vessel thickening and reduced luminal radius, reduced cross-sectional area and reduced intraluminal volume. Thus, caution is advised in comparing

individual differences of pulse pressure height or blood velocity between participants, who may differ in vascular integrity due to age or disease.

Cardiac contractility, or the vigour with which the heart contracts, is determined by the magnitude of intraventricular pressure that is generated during systole and hence arterial blood acceleration. Multiple factors in turn can potentially influence contractility. In *ex vivo* experimental preparations, abrupt increases in afterload, that is, the pressure that the heart must work against to eject blood, can cause a small increase in contractility (the Anrep effect). Under normal conditions blood pressure is the primary determinant of afterload and its impact on cardiac function is to reduce stroke volume and not contractility (Mahler et al., 1975). Likewise, under normal conditions changes of peripheral vascular resistance influence blood pressure and stroke volume but do not influence contractility (Chemla et al., 1996). Preload, which is the amount of stretch experienced by cardiac muscle cells at the end of diastole, will increase contractility due to the length–tension relationship of muscle (Frank–Starling mechanism). Ventricular filling in turn is dependent on venous blood pressure and the rate of venous return. For typical psychophysiology experiments in healthy participants obtained during physical inactivity, the primary modifier of preload is respiration due to cyclic changes of intrathoracic pressure and the volume of venous return during diastole. Respiration is also associated with low-frequency variation of heart rate (Angelone & Coulter Jr., 1964) mediated primarily via vagal tone (Borovkova et al., 2022). A premature ventricular contraction (PVC) can lead to a significant reduction of preload. In the provided software, these beats can be identified and manually removed. Increased heart rate causes an increase

in contractility (the Bowditch effect) (Balcazar et al., 2018; Richmond et al., 1975). In a physically inactive person this is due mainly to reduced parasympathetic drive. The other main determinant of increased contractility (inotropy) as well as accelerating heart rate (chronotropy) is elevated sympathetic drive to the heart. Thus, measures to account for sympathetic effects of heart rate could potentially covary with effects on contractility. However, sympathetic chronotropy is a weak effect for a person at physical rest. To summarize, after adjusting for changes of heart rate and respiration and removing PVCs, measured contractility is a particularly useful variable of interest for tracking what is primarily sympathetic drive to the heart in psychophysiological studies of healthy non-medicated, physically stationary participants.

### 1.1.3 | Modelling the impedance signal

In the arm, peak blood velocity occurs approximately 100ms and peak acceleration occurs 50ms after aortic valve opening. In the following and Table 1, we summarize the relationship between flow, TREV measures and impedance derivatives (for details see Bernstein, 2009). With TREV, impedance  $Z$  is proportional to blood flow velocity. To estimate the magnitude of contractility with TREV, we first take the derivative of velocity  $dZ/dt$  measured in units of  $\Omega/s^2$ . Note that  $dZ/dt$  reaches a maximum around 50–60ms, in close correspondence to the peak acceleration of measured flow after aortic valve opening. The magnitude of this peak can be estimated by taking the derivative of acceleration (in engineering, this is known as ‘jerk’), ( $d^2Z/dt^2$ ), in  $\Omega/s^3$ . This value is proportional to the strength at which the acceleration is generated, which occurs soon after the aortic valve opens, and reflects the contractility-dependent maximal end systolic isovolumic ventricular pressure. Critically, the derivative of acceleration is insensitive to afterload effects such as blood pressure whereas flow velocity is sensitive to afterload effects. As noted above, the magnitude of  $d^2Z/dt^2$  will vary with

heart rate and respiration, which can be measured and accounted for by modelling. In addition to contractility, stroke volume can also be calculated by integrating the normalized complete acceleration curve. This estimate depends on systolic flow time and velocity and is thus sensitive to afterload (blood pressure). A previous validation study demonstrated good correlation between cardiac MRI stroke volume and an impedance measured along the brachial artery of the arm (Bernstein et al., 2015).

The key advantage of TREV for estimating contractility is that the measure is based on blood flow through the linear axially oriented segments of the radial (and ulnar) artery. Contrast this simple arterial geometry with the multi-oriented flow directions in the heart, aortic arch and heavily branching thoracic vasculature that underlie ICG measurements (Trakic et al., 2010; Wang & Patterson, 1995). The complex arterial geometry within the thorax limits the ability to use  $d^2Z/dt^2$  of the ICG signal as a reliable estimator of proximal aorta blood acceleration and hence contractility (Kauppinen et al., 1998; Kosicki et al., 1986). Instead, the most commonly employed ICG estimate of contractility is PEP, an electromechanical time interval measure dependent on the temporal precision of estimating the b-point. TREV estimates are generated without this difficult temporal estimation. Because of the sharpness of the  $dZ/dt$  and  $d^2Z/dt^2$  waveforms, it is possible to estimate directly heart rate from the TREV signal, obviating the need for an independent measure of heart rate by EKG. This capability is included in the Jupyter software described in the accompanying Appendix S1. To account for the influence of respiration and heart rate on contractility, the methodology presented below used a respiratory belt and EKG. These independent timeseries can be fed into our software for modelling out respiration or heart rate effects. Alternatively, we added to the Jupyter software the capability of deriving the respiratory cycle and heart rate directly from  $Z$  waveforms, obviating the need for independent measurements. As with other bio-impedance measurements recorded through surface electrodes, TREV is exceptionally sensitive to motion artefact of the arm. The quality of the recordings will vary as a function of skin turgor and the quality of the electrodes. Impedance  $Z$  depends on the distance between electrode pairs. While the distance can be adjusted to maximize signal-to-noise in an individual, it should be standardized within an individual for repeated-measures experiments. The system described below, with the addition of appropriate patch panel filters, is fMRI-compatible and scans can be obtained in axial or coronal sections. Additional information on the mathematical derivation of contractility, the effect of arterial compliance and extension to estimations of stroke volume are available as a supplement that accompanies the Jupyter software described in the

**TABLE 1** Relationship between arterial blood flow, impedance and units.

Axial blood flow	Impedance along the radial artery <sup>a</sup>	Units	Comments
None	$Z$	$\Omega$	Time invariant
Velocity	$Z$	$\Omega/s$	Time varying
Acceleration	$dZ/dt$	$\Omega/s^2$	
Peak acceleration	$d^2Z/dt^2$	$\Omega/s^3$	Contractility

<sup>a</sup>Assumes no change in blood volume or arterial gas concentration.



Appendix S1, and available at <https://github.com/caitgregory/SCOT>.

## 1.2 | Changes of cardiac contractility with isometric force production

In this section, we demonstrate changes in TREV measures of contractility (after adjusting for variation associated with heart rate and respiration) associated with the production of brief isometric force of maximum hand grip strength obtained for either hand. Using repeated measures of short duration grips, we observed evidence suggesting there is the development of an anticipatory change in contractility prior to grip onset, consistent with allostatic regulation by the autonomic nervous system (McEwen & Wingfield, 2003).

## 2 | METHOD

### 2.1 | Participants and experimental overview

Thirty-one young healthy humans (mean age = 23.4, 19 females) provided informed consent in accordance

with the University of California, Santa Barbara (UCSB) Institutional Review Board. Participants self-reported no cardiovascular abnormalities. One participant was excluded due to excessively noisy data, leaving a final sample of  $n = 30$ . Participants were compensated \$10/h plus a potential \$10 bonus depending on task performance (see Grip task below).

Participants performed two blocks of a 2-s duration maximum Grip task (see Grip task), each block corresponding to three sequential grips of one hand and then the other (with hand order randomized across subjects). Three simultaneous physiological timeseries were recorded during each block. The first timeseries was time-varying cardiac impedance acquired with TREV where electrodes were attached to the forearm contralateral to the hand administering grips (Figure 2). The second timeseries was a standard electrocardiogram (EKG). The last timeseries recorded the continuous respiration cycle with an abdominal belt.

### 2.2 | Recording apparatus

TREV colloid strip electrodes (BIOPAC EL526), each measuring  $1.5 \times 16.5$  cm and connected by a 15 cm cable were attached to the forearm. In participants with smaller

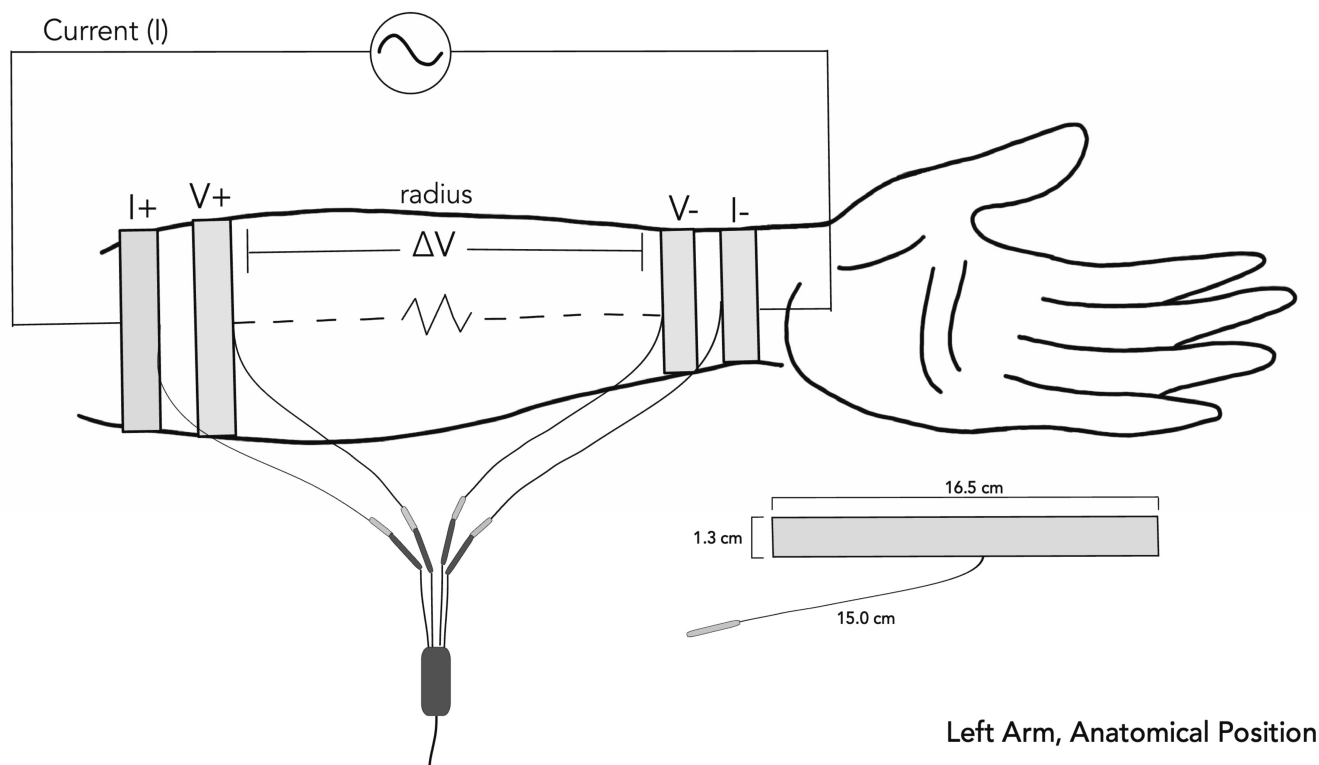


**FIGURE 2** Electrode placement of trans-radial electrical bioimpedance velocimetry system. Four electrodes placed on the forearm; two outer current electrodes ( $I+$  and  $I-$ ) and two inner voltage sensing electrodes ( $V+$  and  $V-$ ).  $I+$  and  $I-$  create an alternating current field ( $I$ ) through the forearm, and any changes in forearm impedance are directly correlated with changes in voltage  $\Delta V$  between  $V+$  and  $V-$ .

wrist sizes the distal two electrodes on the forearm can be trimmed so that they do not wrap over themselves when data are obtained during MRI. A simple skin cleaning procedure, without use of an abrasive exfoliant or application of a salt gel was used (see General Procedure). The electrodes were amplified by an NICO100D (BIOPAC Systems, Inc.) smart amplifier. A current field is applied across the forearm by means of a constant magnitude, high-frequency (50–100 kHz) low-amplitude alternating current (4 mA RMS). The constant current ( $I$ ) is introduced through the two outer electrodes ( $I+$  and  $I-$ ) and the resulting voltage ( $V$ ) is measured via the inner electrodes ( $V+$  and  $V-$ ). Using Ohm's Law, we can use the voltage differential  $V$  and applied current  $I$  to calculate impedance  $Z$ :

$$Z(t) = \frac{V(t)}{I(t)}$$

Here,  $I$  and  $V$  are the root mean square values of the known current and measured voltage. Because the magnitude of the current  $I$  is constant, any change in voltage  $V$  over time will vary in direct proportion to changes in impedance  $Z$ . This method allows us to capture moment-to-moment fluctuations in bioimpedance, reported as  $\Omega/s$  rather than  $\Omega$ .

Electrocardiogram electrodes were amplified by an ECG100D (BIOPAC Systems, Inc.) smart amplifier. Respiration cycle was recorded using a TSD221-MRI (BIOPAC Systems, Inc.) respiration belt. Force exerted in the Grip task was recorded using an SS56L (BIOPAC Systems, Inc.) grip bulb. All continuous signals were integrated using an MP160 (BIOPAC Systems, Inc.) amplifier and processed online using BIOPAC AcqKnowledge software (BIOPAC Systems, Inc.). Visual stimuli were presented on a 21" monitor using Microsoft PowerPoint. Offline preprocessing of recorded timeseries was conducted using the Moving Ensemble Analysis Pipeline (MEAP) and MATLAB (Cieslak et al., 2018). Bayes models were fitted using No U-Turn sampling (NUTS) Hamiltonian Monte Carlo, fitted with PyMC3 Python3 functions (Salvatier et al., 2016).

## 2.3 | General procedure

All data were recorded in a single session lasting approximately 45 min (including initial equipment setup). Participants first washed their hands and forearms with water and regular soap to remove dirt or oily residues then pat dry. In a private setup room, an experimenter then placed four TREV electrodes on the forearm contralateral to the grip hand of the first block (see Grip task). Two electrodes were placed ventrally on the distal region of the forearm, just below where the wrist meets the hand.

Then, two electrodes were placed on the proximal region of the forearm, just below where the elbow meets the forearm (Figure 2). Each electrode pair was spaced 1 cm apart. TREV electrodes are bioimpedance strip electrodes (BIOPAC EL526 – size  $1.3 \times 16.5$  cm). These electrodes establish circumferential equipotential lines at the four electrode locations.

The experimenter placed two EKG electrodes on the participant's chest: one below the right collarbone and one where the deltoid meets the chest (without any skin cleaning). Participants were then brought to the testing room where the experimenter connected electrodes to the associated amplifiers, applied a respiration belt around the participant's abdomen and directed participants to sit at the testing table 3 feet from a computer screen. Once seated, participants were taught how to properly hold and squeeze the grip bulb, with the tubing facing down and in a manner that involved the whole hand. Participants were also instructed to maintain the same posture and to keep their arms relaxed, still, and in the same positioning on the table throughout the entirety of the experiment.

## 2.4 | Grip task

Prior to collecting experimental data, participants were first instructed to grip the bulb as hard as possible with each hand to obtain their maximal force. During these trials the participants' maximum forces were recorded and used as (max thresholds). The experimenter then explained the experimental protocol, which is depicted in Figure 3. The protocol consisted of two blocks of three trials, gripping with the opposite hand in each block (block-hand order was determined with uniform ( $p = .50$ ) probability for each participant). Prior to the start of the first block of trials, participants were instructed to sit idly for 3 min to acclimate to the exam room. The experimenter then quietly entered the room to start the physiological recording and associated computer task. Once the experiment started, the experimenter departed the room. Trials began with an on-screen countdown timer, where participants were instructed to look at the screen during a 2-min rest period. At the end of the rest period, a 'go' cue would appear, signalling to the participants to squeeze the bulb maximally for 2 s. This short duration grip has previously been shown to minimally recruit peripheral vascular autonomic responses (Lott et al., 2002). The generated force was recorded covertly throughout the trial to determine off-line if participants had achieved their prior max threshold. After the 2 s passed, the countdown period of the next trial's rest period then began. This cycle continued for two more grips. At the end of the third trial on each block, a timer counted down to a visual stimulus

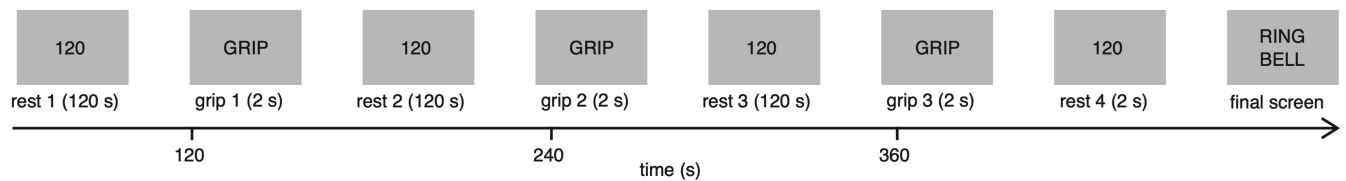


FIGURE 3 Within-block timing of Grip task and rest. This structure was performed for each hand.

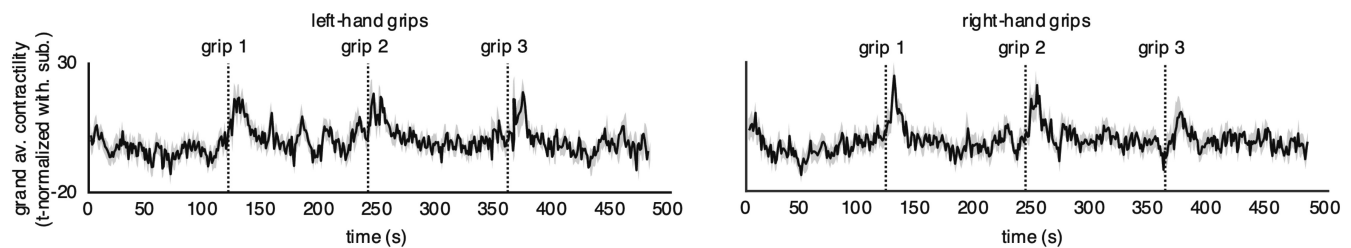


FIGURE 4 Grand average time series of contractility across participants for left- and right-hand blocks of trials.

that instructed participants to ring a bell to alert the experimenter that they had finished. Each of the three trials was therefore preceded and followed by a 2-min rest. To incentivize participants to grip with maximum strength, we imposed a bonus system, whereby participants who reached a threshold of  $\pm 0.04 \text{ kg/m}^2$  of their hand-specific max thresholds on all three grips would win a \$10 bonus. The experimenter disclosed this rule to participants after recording the max thresholds and did not inform participants if they had achieved the bonus until after all testing was completed. After completing the first block, the experimenter transferred the TREV electrodes to the other arm and the Grip task was repeated. Participants were provided with performance feedback after all trials had been completed.

## 2.5 | Cardiovascular preprocessing

During recording, the AcqKnowledge software was used to apply an online lowpass filter (max cutoff = 20 Hz) to the raw impedance timeseries  $Z(t)$  recorded by the TREV electrodes. From this the same software was used to generate a continuous timeseries  $dZ/dt$  (acceleration) and  $d^2Z/dt^2$  (peak-acceleration = contractility). The raw contractility timeseries was then imported together with the raw EKG and respiration timeseries to the MEAP software for minimal offline processing. MEAP first automatically labelled the R-peaks of the EKG timeseries, which we used as an index for the moment in time to define each individual heartbeat. We next used these R-peak time indices to extract epochs spanning  $\pm 350 \text{ ms}$  around each heartbeat from the raw contractility timeseries (contractility epochs). MEAP also computed estimates of heart rate at each beat from the R-peaks. MEAP

outputs were then transferred to MATLAB, where the maximum amplitude in each contractility epoch was computed as an estimation of each heartbeat's contractility (beat-wise contractility timeseries). Then, separately for each subject, and each block, we conducted an additional regression procedure (Dundon et al., 2020; Dundon et al., 2021) to remove the additional confounding effects of heart rate and respiration from the beat-wise contractility timeseries. Using a multiple regression model, we regressed the vector beat-wise contractility as a function of an intercept and three regressors: (i) the phase of respiration at each heartbeat, (ii) the amplitude of respiration at each heartbeat and (iii) the heart rate at each heartbeat. To down-sample each regressor to beat-wise estimates, we used the value from raw timeseries closest to the time of each R-peak. We added the estimated intercept to the residuals from this model as the 'residualized' contractility timeseries, that is, with the effects of the above three regressors removed. Given both between-subject and within-subject variation in heart rate, we next applied temporal resampling of each block's residualized timeseries to allow meaningful comparisons across participants. For this, we used one-dimensional linear interpolation across time to recreate residualized timeseries sampled at equal time intervals. Specifically, we took 479 estimates, spaced exactly 1 s apart, from 2 s post-block onset until 480 s post-block onset (interpolated contractility timeseries). Finally, these interpolated contractility timeseries were normalized as a  $t$ -statistic, that is, each interpolated contractility estimate expressed as a  $t$ -statistic relative to the timeseries's remaining 478 values. We refer to this  $t$ -statistic-normalized timeseries from now on as the 'contractility' timeseries. A grand average contractility timeseries across participants, separately for each block, is presented in Figure 4.

## 2.6 | Bayesian modelling framework

The primary objective of this analyses was to determine whether TREV could reliably capture increases in group-level contractility that corresponded to the events in the Grip task, either in response to, or in anticipation of a grip. We additionally required evidence robust to type I error, given our sample size ( $n = 30$ ). Given these requirements, we accordingly used a hierarchical Bayesian framework which hypothesized that the ( $n = 30$ ) group distribution of contractility estimates at each timepoint ( $t$ ) formed a Student's  $T$  distribution,  $T(t) \sim \text{Student's } T(\mu(t), \text{sig}(t), \nu)$ . In doing so we obviate the need to correct for multiple comparisons inherent with null hypothesis testing. We formally considered contractility to have increased beyond baseline at a given moment where the estimated mean of a timepoint's distribution ( $\mu(t)$ ) credibly exceeded the mean across all timepoints ( $M_{\text{mu}}$ ).  $M_{\text{mu}}$  is itself fitted in the same model as the mean of a hierarchical Gaussian distribution ( $G_{\text{mu}}$ ) which constrains estimates of each  $\mu(t)$  by serving as their prior ( $G_{\text{mu}} \sim N(M_{\text{mu}}, S_{\text{mu}})$ ). This hierarchical relation between  $M_{\text{mu}}$  and each measure of  $\mu(t)$  minimizes type I risk. Specifically, Bayes theorem ascribes joint probabilities to both the prior and the observed data in posterior estimates, meaning that outlier datapoints will have minimal impact on broader estimates. For example, if most values for  $\mu(t)$  are within a tight range (as we would expect in a data set of contractility values with long rest periods between grips), the hierarchical distribution will be characterized by a more certain mean and low variance (low value of  $S_{\text{mu}}$ ), which would then serve as a strict prior on  $\mu(t)$  estimates, biasing them towards the group mean (i.e. a nail that stands out gets hammered in). This hierarchical framework therefore requires strong evidence before any  $\mu(t)$  is formally accepted as a credible departure. In other words, in a context requiring multiple hypothesis tests, the hierarchical Bayesian framework imposes an adjustment to the level of evidence needed for credible effects, where the data itself determine that level of adjustment instead of an arbitrary criterion (e.g. Bonferroni).

We fitted a hierarchical model separately for blocks where grip was administered with the right and left hand. In each case, the specific free parameters of our model were  $\mu(t)$  and  $\text{sigma}(t)$ , that is, the 479 timepoint-specific mean and standard deviation parameters for group-level SNS distributions at each timepoint across each block. We did not fit the  $\nu$  parameter hierarchically and assigned it the same uninformed prior ( $\nu = 1$ ) in each model. As mentioned above, each  $\mu(t)$  parameter was constrained by a hierarchical Gaussian distribution ( $G_{\text{mu}}$ ) with free parameters  $M_{\text{mu}}$  and  $S_{\text{mu}}$  corresponding respectively to its mean and standard deviation.  $M_{\text{mu}}$  was assigned an uninformed

Gaussian prior,  $N(0, 1)$ , while  $S_{\text{mu}}$  was assigned an uninformed half-Gaussian prior (forcing values to be positive), half  $N(1)$ . Each  $\text{sigma}(t)$  was also constrained by hierarchical Gaussian distribution ( $G_{\text{sigma}}$ ), which respectively used an uninformed Gaussian and half-Gaussian prior for its two free parameters, that is, its mean ( $M_{\text{sigma}} \sim N(0, 1)$ ) and standard deviation ( $S_{\text{sigma}} \sim \text{half } N(1)$ ). We formally compared each  $\mu(t)$  posterior with that of the  $M_{\text{mu}}$  by computing the minimum-width Bayesian credible interval (highest density interval (HDI)) of  $\mu(t) - M_{\text{mu}}$  and only considered strong evidence of a departure at each timepoint, that is, where resulting HDIs did not contain zero.

Contractility timeseries were z score normalized prior to fitting across all participants. Each model's posterior distributions were sampled across four chains of 5000 samples (20,000 total), after burning an initial 5000 samples per chain to tune the sampler's step-size to reach 0.95 acceptance. We estimated HDIs using the default setting in the arviz package (Kumar et al., 2019).

## 2.7 | Sliding window rate of change

We performed a sliding window deterministic regression to enumerate the rate of change in contractility at each point in our timeseries. At each timepoint we estimated the rate of change in contractility over the ensuing 20s of the timeseries. Specifically, for each timepoint( $t$ ) we fitted a distribution of coefficients ( $B(t)$ ), containing 5000 coefficients ( $b(k)$ ), where each  $b(k)$  estimated the relation between an arbitrary time vector  $[1, \dots, 20]$  and independent draws from the proceeding 20 posteriors of  $\mu$ , that is, the 20-element vector  $[[\mu(t)](k), \dots, [\mu(t+19)](k)]$ . To identify credibly positive rates of change, we tested whether 97% of each deterministic distribution ( $B(t)$ ) was above zero.

## 3 | RESULTS

We tested whether a thorax-independent monitor of cardiac impedance (TREV) could reliably describe fluctuations in cardiac contractility that credibly exceed baseline as human participants perform a task known to increase cardiovascular sympathetic demand (Stanek & Richter, 2016; Stanek & Richter, 2021). Thirty participants completed both blocks of three incentivized max-intensity grips, with rest periods of 2 min both between each grip and following the final grip. Participants showed strong motivation to grip at maximum intensity, supported by 29 of 30 achieving a bonus payment (contingent on beating their predetermined max threshold) with at least one



hand, and 21 of 30 achieving the bonus payment with both. Figure 5 depicts exemplar contractility for two heartbeats from a single subject, one in the rest phase prior to the second grip with their right hand, and another in the grip's immediate aftermath.

After linear resampling to temporally align contractility across participants and normalizing each block separately as a  $t$ -statistic, group-level contractility in temporal approximation to each grip was assessed. The results of the hierarchical Bayesian model fitted to contractility timeseries accompanying left-hand grips are depicted in the left panel of Figure 6. TREV reliably captured contractility exceeding baseline following grips with the left hand. Left-hand grips were accompanied by credible baseline departure in seconds after grip onset at grip 1: [11, 12, 13, 15], grip 2: [-8, 5, 10, 11, 13] and grip 3: [8, 12, 13, 14, 15]. Each grip was therefore accompanied by at least 4 individual seconds of credible baseline departure. Departures mostly followed the grips and never followed a grip by more than 15 s. Each grip was associated with at least two consecutive seconds of baseline departure, with grip 3 associated with the longest sustained peak contractility (four consecutive points).

The results of the hierarchical Bayesian model fitted to contractility timeseries accompanying right-hand grips are depicted in the right panel of Figure 6. Right-hand grips were accompanied by credible baseline departure after

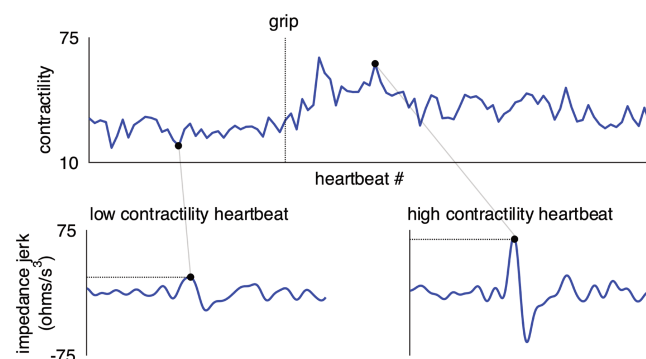


**FIGURE 5** Top row is a sample timeseries of contractility estimated at 100 heartbeats. Bottom row shows how contractility is estimated from impedance jerk timeseries at two single heartbeats.

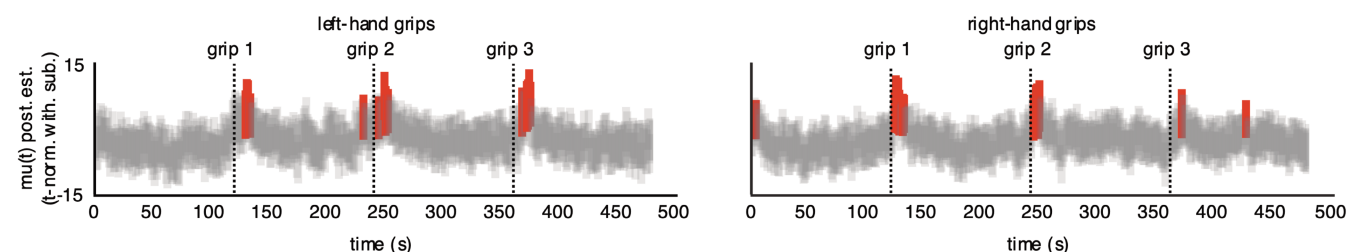


**FIGURE 6** Results of hierarchical Bayesian model depicting credible departures from baseline contractility (in red) for left- and right-hand grips.

grip onset (in seconds) for grip 1: [-114, 5, 6, 7, 8, 9, 12, 13], grip 2: [4, 5, 6, 7, 8, 9] and grip 3: [11, 66]. Discounting the two outliers (preceding grip 1 and following grip 3), each grip was therefore accompanied by at least 1 s of credible baseline departure. Departures all followed the grips and never followed a grip by more than 13 s. Grip 2 was associated with the longest sustained peak contractility (six consecutive points). TREV again appeared to reliably capture contractility exceeding baseline following grips with the right hand, although a pair of outliers were present and the duration of peak contractility seemed to abate over the course of the three grips.

### 3.1 | Sliding window rate of change

As depicted in Figure 7, for both the left- and right-hand grips, the rate of change estimate over a sliding 20-s time window was credibly positive at numerous timepoints in the series preceding each grip. For the left hand, the earliest of these credible pre-grip changes occurred at  $t=62$ , that is, 58 s prior to the first grip; at  $t=185$ , that is, 55 s prior to the second grip; and at  $t=349$ , that is, 11 s prior to the third grip. For the right hand, the earliest of these credible pre-grip changes occurred at  $t=45$ , that is, 75 s prior to the first grip; at  $t=178$ , that is, 62 s prior to the second grip; and at  $t=348$ , that is, 12 s prior to the third grip. Interestingly, therefore, we observed a trend in both hands, whereby the rate of change became credibly positive much closer to the initiation of the grip by the third grip, consistent with the allostatic principle of participants learning task requirements and reserving a potentially expensive increase in cardiac contractility until the time it was most critically needed.

## 4 | DISCUSSION

There is expanding interest across multiple human research disciplines in robustly capturing event-related perturbations of the sympathetic response in the heart. Consequently, there is a need for new assays of cardiac

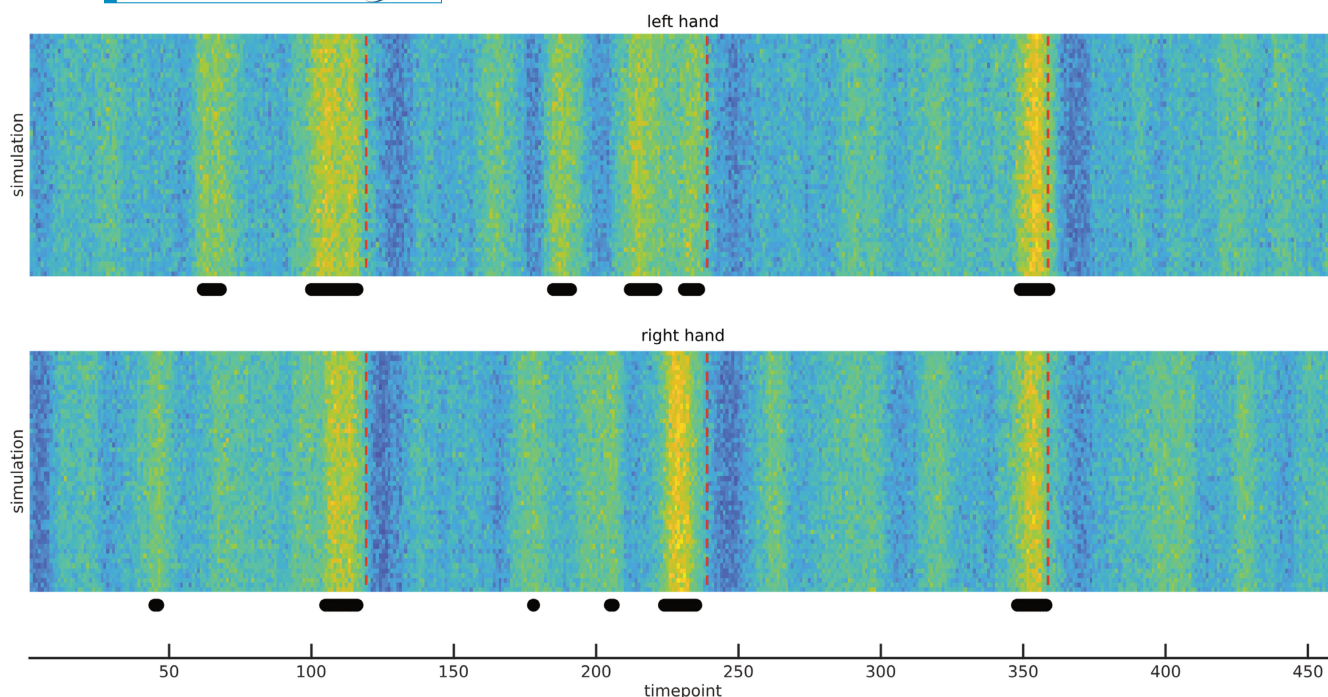


**FIGURE 7** Sliding window rate-of-change. Each column of raster plots are 50 samples from distributions of regression coefficients measuring change in contractility over next 20-s window. Yellow colours are positive (increasing contractility). Markers below each panel reflect timepoints when 97% of distribution is positive, that is, credibly positive increase in contractility.

contractility that both reduce preparatory requirements and offer increased signal strength in the face of background noise. In this study we used a novel trans-radial electrical bioimpedance velocimetry device (TREV), attached to the forearm of human participants, and investigated whether it could reliably capture changes in group-level contractility that corresponded to events known to increase sympathetic drive, a max Grip task (Grip task). We observed that TREV electrodes can be applied relatively quickly with minimal training and preparation, and can even be repositioned (from one arm to the other) efficiently between blocks of a task. We further observed TREV to register visually identifiable beat-to-beat signals from the radial and ulnar artery corresponding to the second derivative of the measured impedance wave. In preprocessing, we could readily control for potential confounding effects of respiratory activity and heart rate on beat-wise contractility timeseries. We observed the contractility timeseries to reliably depart baseline at key events in the Grip task. Remarkably, these departures were seen at the single-trial level across participants (i.e. without averaging across trials). We therefore conclude that TREV offers an exciting development in cardiac autonomic research for human researchers interested in event-related capture of cardiac contractility.

We employed a data-driven analysis within a hierarchical Bayesian framework, which used the entire timeseries of data recorded across sessions, to determine

when contractility estimated by TREV credibly exceeded baseline fluctuations. The primary advantage of this framework is that it removed all need to impose arbitrary criteria on grip events or contractility activity, that is, a priori deciding epochs around task events to refine analysis, or a priori deciding a criterion that constituted 'credibly exceeding baseline'. The analysis was not assisted by any averaging across events to reduce signal to noise. The hierarchical Bayesian framework also imposed conservativeness with respect to credible departures from baseline across a large number of hypothesis tests. Despite the moderate sample size, the analytic approach nonetheless revealed reliable group-level increases in contractility at each of the six grips executed by participants. These increases were corroborated with post hoc confidence intervals of contractility relative to individual baselines. We propose that the observed significant change in contractility to the physical challenge imposed by the Grip task is driven primarily by a sympathetic response (as heart rate and respiration were adjusted for). Note that the heart rate adjustment might attenuate the magnitude of the contractility estimate if there is concomitantly strong sympathetic chronotropy. The other potential modifier of the measurement would be an acute rise in blood pressure mediated through sympathetic alpha stimulation to the vascular bed of muscles. However, there are several factors that make this unlikely. We used a brief isometric grip force paradigm where a bulb was squeezed maximally for only

2s. Previous studies demonstrating a blood pressure effect have relied entirely on sustained isometric force production (El Sayed et al., 2016; Gandevia & Hobbs, 1990; MacDougall et al., 1992). In contrast, short duration grip has been used to avoid changes of blood pressure (Lott et al., 2002). Furthermore, a combined study of sustained isometric grip force, blood pressure and muscle sympathetic nerve activity demonstrated that blood pressure rises slowly; mean arterial pressure increased only ~7% over the first 15s after grip onset (El Sayed et al., 2016). The changes observed with TREV are far greater in magnitude and develop more rapidly. More importantly, blood pressure changes should primarily influence afterload and stroke volume, but not peak acceleration of flow as measured by TREV. Given these points, the main effect on this measurement is likely to be a sympathetic inotropic effect to the heart, consistent with motivational intensity theory. This theory posits that the sympathetic response should scale with the level of task difficulty, an effect which has been observed in both cognitive and Grip tasks (see Richter et al., 2016, for a review).

Note that our criterion for baseline was the average value across all datapoints in the timeseries, which theoretically incorporates all preparatory increases in sympathetic activity leading up to grip execution. When we employed a slope-based analysis strategy, we additionally observed credible anticipatory changes of contractility just prior to grip onset for all trials and with either hand. This observation is consistent with the role of the sympathetic nervous system in allostatic regulation, providing just enough input and just in time (McEwen & Wingfield, 2003).

In conclusion, we observed that TREV reliably captures contractility increases to individual events. Capturing these contractility changes has the potential to greatly contribute towards improving our knowledge of how humans synchronize autonomic regulation while monitoring broader state information, allowing us to develop more holistic technologies for human-machine integration that can assist with situational awareness, manoeuvrability and decision making.

## AUTHOR CONTRIBUTIONS

**Alexandra Stump:** Data curation; investigation; writing – original draft. **Caitlin Emma Gregory:** Formal analysis; methodology; resources; software; writing – original draft. **Viktoriya Babenko:** Conceptualization; data curation; investigation. **Elizabeth Rizer:** Data curation; investigation; resources. **Tom Bullock:** Methodology; resources; software; supervision; validation. **Alan Macy:** Resources; software; validation. **Barry Giesbrecht:** Funding acquisition; methodology; resources; supervision; writing – review and editing. **Scott T. Grafton:** Conceptualization;

formal analysis; funding acquisition; project administration; resources; supervision; writing – original draft. **Neil M. M. Dundon:** Formal analysis; investigation; methodology; resources; software; supervision; validation; writing – original draft.










## ACKNOWLEDGEMENTS

In memory of Don Bernstein. Supported by the Institute for Collaborative Biotechnologies under Cooperative Agreement W911NF-19-2-0026, contract W911NF-19-D-0001 and grant W911NF-16-1-0474, all from the Army Research Office. The content of the information does not necessarily reflect the position or the policy of the Government and no official endorsement should be inferred. Open Access funding enabled and organized by Projekt DEAL.

## DATA AVAILABILITY STATEMENT

Jupyter notebook for deriving cardiac contractility from impedance measurements available from our github <https://github.com/caitgregory/SCOT>. Also see Appendix S1 of this manuscript for a detailed tutorial. Users can fully test or replicate pipeline by downloading an example data, link in <https://github.com/caitgregory/SCOT/blob/main/tutorial.md>. Any other data that support the findings of this study are available from the corresponding author upon reasonable request.

## ORCID

Alexandra Stump  <https://orcid.org/0000-0003-4361-0610>  
 Caitlin Gregory  <https://orcid.org/0009-0002-8285-081X>  
 Viktoriya Babenko  <https://orcid.org/0000-0002-0510-8016>  
 Elizabeth Rizer  <https://orcid.org/0000-0002-5833-4471>  
 Tom Bullock  <https://orcid.org/0000-0002-8551-905X>  
 Alan Macy  <https://orcid.org/0000-0001-9808-9143>  
 Barry Giesbrecht  <https://orcid.org/0000-0002-1976-1251>  
 Scott T. Grafton  <https://orcid.org/0000-0003-4015-3151>  
 Neil M. Dundon  <https://orcid.org/0000-0001-6246-1775>

## REFERENCES

- Angelone, A., & Coulter, N. A., Jr. (1964). Respiratory sinus arrhythmia: A frequency dependent phenomenon. *Journal of Applied Physiology*, 19(3), 479–482. <https://doi.org/10.1152/jappl.1964.19.3.479>
- Balcazar, D., Regge, V., Santalla, M., Meyer, H., Paululat, A., Mattiazzi, A., & Ferrero, P. (2018). SERCA is critical to control the Bowditch effect in the heart. *Scientific Reports*, 8, 12447. <https://doi.org/10.1038/s41598-018-30638-9>
- Bernstein, D. P. (2009). Impedance cardiography: Pulsatile blood flow and the biophysical and electrodynamic basis for the stroke volume equations. *Journal of Electrical Bioimpedance*, 1(1), 2–17. <https://doi.org/10.5617/jeb.51>
- Bernstein, D. P., Henry, I. C., Banet, M. J., & Dittrich, T. (2012). Stroke volume obtained by electrical interrogation of the



- brachial artery: Transbrachial electrical bioimpedance velocimetry. *Physiological Measurement*, 33(4), 629–649. <https://doi.org/10.1088/0967-3334/33/4/629>
- Bernstein, D. P., Henry, I. C., Lemmens, H. J., Chaltas, J. L., DeMaria, A. N., Moon, J. B., & Kahn, A. M. (2015). Validation of stroke volume and cardiac output by electrical interrogation of the brachial artery in normals: Assessment of strengths, limitations, and sources of error. *Journal of Clinical Monitoring and Computing*, 29(6), 789–800. <https://doi.org/10.1007/s10877-015-9668-9>
- Blascovich, J. (2013). Challenge and threat. In A. J. Elliot (Ed.), *Handbook of approach and avoidance motivation* (pp. 431–445). Psychology Press.
- Borovkova, E. I., Prokhorov, M. D., Kiselev, A. R., Hramkov, A. N., Mironov, S. A., Agaltsov, M. V., Ponomarenko, V. I., Karavaev, A. S., Drapkina, O. M., & Penzel, T. (2022). Directional couplings between the respiration and parasympathetic control of the heart rate during sleep and wakefulness in healthy subjects at different ages. *Frontiers in Network Physiology*, 2, 942700. <https://doi.org/10.3389/fnetp.2022.942700>
- Chemla, D., Demolis, P., Thyrault, M., Annane, D., Lecarpentier, Y., & Giudicelli, J. F. (1996). Blood flow acceleration in the carotid and brachial arteries of healthy volunteers: Respective contributions of cardiac performance and local resistance. *Fundamental and Clinical Pharmacology*, 10(4), 393–399. <https://doi.org/10.1111/j.1472-8206.1996.tb00591.x>
- Chuang, M. L., Douglas, P. S., Bisinov, E. A., & Stein, J. H. (2002). Effect of cardiac cycle on ultrasound assessment of endothelial function. *Vascular Medicine*, 7(2), 103–108. <https://doi.org/10.1191/1358863x02vm425oa>
- Cieslak, M., Ryan, W. S., Babenko, V., Erro, H., Rathbun, Z. M., Meiring, W., Kelsey, R. M., Blascovich, J., & Grafton, S. T. (2018). Quantifying rapid changes in cardiovascular state with a moving ensemble average. *Psychophysiology*, 55(4), e13018. <https://doi.org/10.1111/psyp.13018>
- Dundon, N. M., Garrett, N., Babenko, V., Cieslak, M., Daw, N. D., & Grafton, S. T. (2020). Sympathetic involvement in time-constrained sequential foraging. *Cognitive, Affective, & Behavioral Neuroscience*, 20(4), 730–745. <https://doi.org/10.3758/s13415-020-00799-0>
- Dundon, N. M., Shapiro, A. D., Babenko, V., Okafor, G. N., & Grafton, S. T. (2021). Ventromedial prefrontal cortex activity and sympathetic allostasis during value-based ambivalence. *Frontiers in Behavioral Neuroscience*, 15, 615796. <https://doi.org/10.3389/fnbeh.2021.615796>
- El Sayed, K., Macefield, V. G., Hissen, S. L., Joyner, M. J., & Taylor, C. E. (2016). Rate of rise in diastolic blood pressure influences vascular sympathetic response to mental stress. *The Journal of Physiology*, 594, 7465–7482. <https://doi.org/10.1113/JP272963>
- Gandevia, S. C., & Hobbs, S. F. (1990). Cardiovascular responses to static exercise in man: Central and reflex contributions. *The Journal of Physiology*, 430, 105–117. <https://doi.org/10.1113/jphysiol.1990.sp018284>
- Gramfort, A., Luessi, M., Larson, E., Engemann, D., Strohmeier, D., Brodbeck, C., Goj, R., Jas, M., Brooks, T., Parkkonen, L., & Hämäläinen, M. (2013). MEG and EEG data analysis with MNE-Python. *Frontiers in Neuroscience*, 7, 267. <https://doi.org/10.3389/fnins.2013.00267>
- Green, D., Cheetham, C., Reed, C., Dembo, L., & O'Driscoll, G. (2002). Assessment of brachial artery blood flow across the cardiac cycle: Retrograde flows during cycle ergometry. *Journal of Applied Physiology* (1985), 93(1), 361–368. <https://doi.org/10.1152/japplphysiol.00051.2002>
- Hunter, J. D. (2007). Matplotlib: A 2D graphics environment. *Computing in Science & Engineering*, 9, 90–95. <https://doi.org/10.1109/MCSE.2007.55>
- Kauppinen, P. K., Hyttinen, J. A., & Malmivuo, J. A. (1998). Sensitivity distributions of impedance cardiography using band and spot electrodes analyzed by a three-dimensional computer model. *Annals of Biomedical Engineering*, 26, 694–702. <https://doi.org/10.1114/1.44>
- Kosicki, J., Chen, L. H., Hobbie, R., Patterson, R., & Ackerman, E. (1986). Contributions to the impedance cardiogram waveform. *Annals of Biomedical Engineering*, 14, 67–80. <https://doi.org/10.1007/BF02364649>
- Kumar, R., Carroll, C., Hartikainen, A., & Martin, O. (2019). ArviZ a unified library for exploratory analysis of Bayesian models in Python. *Journal of Open Source Software*, 4(33), 1143. <https://doi.org/10.21105/joss.01143>
- Lott, M. E., Herr, M. D., & Sinoway, L. I. (2002). Effects of transmural pressure on brachial artery mean blood velocity dynamics in humans. *Journal of Applied Physiology* (1985), 93(6), 2137–2146. <https://doi.org/10.1152/japplphysiol.00443.2002>
- MacDougall, J. D., McKelvie, R. S., Moroz, D. E., Sale, D. G., McCartney, N., & Buick, F. (1992). Factors affecting blood pressure during heavy weight lifting and static contractions. *Journal of Applied Physiology* (1985), 73(4), 1590–1597. <https://doi.org/10.1152/jappl.1992.73.4.1590>
- Mahler, F., Ross, J., Jr., O'Rourke, R. A., & Covell, J. W. (1975). Effects of changes in preload, afterload and inotropic state on ejection and isovolumic phase measures of contractility in the conscious dog. *The American Journal of Cardiology*, 35(5), 626–634. [https://doi.org/10.1016/0002-9149\(75\)90048-X](https://doi.org/10.1016/0002-9149(75)90048-X)
- McEwen, B. S., & Wingfield, J. C. (2003). The concept of allostasis in biology and biomedicine. *Hormones and Behavior*, 43(1), 2–15. [https://doi.org/10.1016/S0018-506X\(02\)00024-7](https://doi.org/10.1016/S0018-506X(02)00024-7)
- Miller, J. C., & Horvath, S. M. (1978). Impedance cardiography. *Psychophysiology*, 15(1), 80–91. <https://doi.org/10.1111/j.1469-8986.1978.tb01340.x>
- Obrist, P. A. (1981). *Cardiovascular psychophysiology: A perspective*. Plenum.
- Richmond, D. R., Angus, J. A., Goodman, A. H., & Cobbin, L. B. (1975). The effect of heart rate on indices of myocardial contractility in the dog. *Clinical and Experimental Pharmacology and Physiology*, 2(6), 469–479. <https://doi.org/10.1111/j.1440-1681.1975.tb01852.x>
- Richter, M., & Gendolla, G. H. E. (2009). The heart contracts to reward: Monetary incentives and preejection period. *Psychophysiology*, 46(3), 451–457. <https://doi.org/10.1111/j.1469-8986.2009.00795.x>
- Richter, M., Gendolla, G. H. E., & Wright, R. A. (2016). Three decades of research on motivational intensity theory: What we have learned about effort and what we still don't know. In A. J. Elliot (Ed.), *Advances in motivation science* (Vol. 3, pp. 149–186). Elsevier. <https://doi.org/10.1016/bs.adms.2016.02.001>
- Salvatier, J., Wiecki, T. V., & Fonnesbeck, C. (2016). Probabilistic programming in python using PyMC3. *PeerJ Computer Science*, 2, e55. <https://doi.org/10.7717/peerj-cs.55>
- Sel, K., Osman, D., & Jafari, R. (2021). Non-invasive cardiac and respiratory activity assessment from various human body locations using bioimpedance. *IEEE Open Journal of Engineering in Medicine and Biology*, 2, 210–217. <https://doi.org/10.1109/ojemb.2021.3085482>



- Stanek, J., & Richter, M. (2016). Evidence against the primacy of energy conservation: Exerted force in possible and impossible handgrip tasks. *Motivation Science*, 2(1), 49–65. <https://doi.org/10.1037/mot0000028>
- Stanek, J. C., & Richter, M. (2021). Energy investment and motivation: The additive impact of task demand and reward value on exerted force in hand grip tasks. *Motivation and Emotion*, 45, 131–145. <https://doi.org/10.1007/s11031-020-09862-2>
- Trakic, A., Akhand, M., Wang, H., Mason, D., Liu, F., Wilson, S., & Crozier, S. (2010). Computational modelling of blood-flow-induced changes in blood electrical conductivity and its contribution to the impedance cardiogram. *Physiological Measurement*, 31(1), 13–33. <https://doi.org/10.1088/0967-3334/31/1/002>
- Vack, N. (2023). bioread 3.0.1. Python package index. <https://pypi.org/project/bioread>
- Virtanen, P., Gommers, R., Oliphant, T. E., Haberland, M., Reddy, T., Cournapeau, D., Burovski, E., Peterson, P., Weckesser, W., Bright, J., Van Der Walt, S. J., Brett, M., Wilson, J., Millman, K. J., Mayorov, N., Nelson, A. R. J., Jones, E., Kern, R., Larson, E., ... SciPy 1.0 Contributors. (2020). SciPy 1.0: Fundamental algorithms for scientific computing in Python. *Nature Methods*, 17, 261–272. <https://doi.org/10.1038/s41592-019-0686-2>
- Wang, L., & Patterson, R. (1995). Multiple sources of the impedance cardiogram based on 3-D finite difference human thorax models. *IEEE Transactions on Bio-Medical Engineering*, 42(2), 141–148. <https://doi.org/10.1109/10.341826>

## SUPPORTING INFORMATION

Additional supporting information can be found online in the Supporting Information section at the end of this article.

**Appendix S1.** Jupyter-based signal processing software.

**Figure S1.** Cell 1 GUI.

**Figure S2.** GUI for cell 2. Note the peak threshold is inputted as 0.5. This threshold value helps avoid flutter between acceleration peaks. The participant has a premature ventricular contraction at time 16.5 s (causing a reduction of contractility due to reduced ventricular filling). Also note the onset of MRI scanning at 18 s. Despite the associated MRI noise, acceleration peaks are still visible and robust.

**Figure S3.** Cell 3 GUI. The acceleration time series plotted over time with detected peaks. The user is able to use the slider along the bottom of the graph to scroll through the data and adjust the peak location as needed.

**Figure S4.** Cell 4 GUI. The contractility timeseries plotted over time.

**How to cite this article:** Stump, A., Gregory, C., Babenko, V., Rizor, E., Bullock, T., Macy, A., Giesbrecht, B., Grafton, S. T., & Dundon, N. M. (2024). Non-invasive monitoring of cardiac contractility: Trans-radial electrical bioimpedance velocimetry (TREV). *Psychophysiology*, 61, e14411. <https://doi.org/10.1111/psyp.14411>